J. Fluid Mech. (2024), *vol*. 987, R8, doi:10.1017/jfm.2024.440

Evidence of quasiequilibrium in pressure-gradient turbulent boundary layers

Victor Baxerres[1], **Ricardo Vinuesa**[2] **and Hassan Nagib**[1],†

[1]Illinois Tech (IIT), Chicago, IL 60616, USA

[2]FLOW, Engineering Mechanics, KTH Royal Institute of Technology, Stockholm, Sweden

(Received 14 November 2023; revised 20 March 2024; accepted 24 April 2024)

Two sets of measurements utilizing hot-wire anemometry and oil-film interferometry for flat-plate turbulent boundary layers, exposed to various controlled adverse and favourable pressure gradients, are used to evaluate history effects of the imposed and varying free-stream gradients. The results are from the NDF wind tunnel at Illinois Tech (IIT) and the MTL wind tunnel at KTH, over the range $800 < Re_\tau < 22\,000$ (where Re_τ is the friction Reynolds number). The streamwise pressure-gradient parameter $\beta \equiv (-\ell/\tau_w) \cdot (\partial P_e/\partial x)$ varied between $-2 < \beta < 7$, where ℓ is an outer length scale for boundary layers equivalent to the half-height of channel flow and the radius of pipe flow, and is estimated for each boundary-layer profile; note that τ_w is the wall-shear stress and P_e is the free-stream static pressure. Extracting from each profile the three parameters of the overlap region, following the recent work of Monkewitz & Nagib (*J. Fluid Mech.*, vol. 967, 2023, p. A15) that led to an overlap region of combined logarithmic and linear parts, we find minimum history effects in the overlap region. Thus, the overlap region in this range of pressure-gradient boundary layers appears to be in 'quasiequilibrium'.

Key words: turbulent boundary layers, boundary layer structure, turbulence theory

1. Introduction

A topic within the study of wall-bounded turbulence that has received extensive attention for many decades, due to its significant implications on flow representation and modelling, is the overlap region between the inner or wall region and the outer region of the flow. According to the classical literature, the mean velocity profile in this overlap region follows the well-known logarithmic law (1.1), which contains κ, the von Kármán constant:

$$\bar{U}^+_{x\,OL}(\,y^+ \gg 1 \;\textit{and}\; Y \ll 1) = \frac{1}{\kappa}\ln y^+ + B. \tag{1.1}$$

† Email address for correspondence: nagib@iit.edu

In this equation, $\bar{U}_x$ is the streamwise mean velocity, the '+' superscript indicates that we are using the viscous scaling, and the '*OL*' subscript indicates validity in the overlap region. The independent variable y^+ is the inner-scaled wall-normal coordinate, $y^+ = yu_\tau/\nu$, where u_τ is the friction velocity and ν is the fluid kinematic viscosity. The variable Y is the wall-normal coordinate made dimensionless by the 'outer scale of the flow' ℓ. Since the work of Nagib & Chauhan (2008) the universality of the log law and the von Kármán 'coefficient' have been occasionally challenged or reaffirmed, e.g. see references by George & Castillo (2006), Monkewitz, Chauhan & Nagib (2008), Vinuesa, Schlatter & Nagib (2014), Luchini (2017). More recently, Monkewitz & Nagib (2023) (MN23 from now on) shed additional light on this topic, challenging the knowledge accumulated during the last century. The main point of MN23 is that a more thorough matched asymptotic expansion (MAE) of wall-bounded flows yields an overlap region containing a combination of logarithmic and linear terms of the distance to the wall in (1.2). They arrived at this result by considering in the inner asymptotic expansion a term proportional to the wall-normal coordinate, $O(Re_\tau^{-1})$. Here we will reference this overlap region as 'log+lin', and use $Re_\tau = u_\tau \ell/\nu$, which is the friction Reynolds number with ℓ a characteristic outer length. For consistency with MN23, this ℓ can be thought of as the radius R in pipes, the semiheight in channels, h, or a length scale related to the 99 % boundary-layer thickness δ_{99} in boundary layers:

$$\bar{U}^+_{xOL}(\, y^+ \gg 1 \text{ and } Y \ll 1) = \kappa^{-1} \ln y^+ + S_0 y^+/Re_\tau + B_0 + B_1/Re_\tau. \tag{1.2}$$

Note that in equation (1.2), S_0, B_0 and B_1 are constants. Earlier publications by Yajnik (1970), Afzal & Yajnik (1973), Lee & Moser (2015), Luchini (2017) have considered a linear term in the overlap region of channel and pipe flows. However, unlike MN23, none of them revealed the non-universality of the Kármán constant, or the dependence of the overlap coefficients κ, S_0 and B_0 on the pressure gradient along the flow. In most literature on boundary layers, including for turbulent conditions, the commonly used pressure-gradient parameter is $\beta^* \equiv (-\delta^*/\tau_w) \cdot (\partial P_e/\partial x)$, where δ^* is the displacement thickness, τ_w the wall-shear stress, and P_e is the free-stream static pressure. In order to compare results from developing boundary layers to fully developed flow in channels and pipes, at corresponding pressure gradients, we will use the parameter $\beta \equiv (-\ell/\tau_w) \cdot (\partial P_e/\partial x)$. The outer length scale of all boundary-layer profiles used here, ℓ, is established in the next section. Effects of pressure gradient on boundary layers have often been considered to have 'history effects' on the flow. In particular, several studies have documented flow-history effects on the Reynolds stresses and the wake region of the mean velocity profile (Harun *et al.* 2013; Bobke *et al.* 2017), while other studies have also reported an effect of flow history on the overlap region and its coefficients κ and B (Vishwanathan *et al.* 2023).

Our objective here is to examine whether such history effects are present in the overlap region, or a behaviour more like quasiequilibrium exists when the log+lin overlap is used to analyse well-documented boundary-layer data under conditions of adverse pressure gradient (APG) or favourable pressure gradient (FPG), including strong favourable pressure gradient (SFPG), and, for reference, zero pressure gradient (ZPG). Here, we use 'quasiequilibrium' to signify that the three parameters defining the mean velocity profile in the overlap region between the inner and outer flow are independent of the upstream or history effects experienced by the boundary layer. We also expect that any quasiequilibrium, or diminished history effects, in turbulence quantities may be delayed past the establishment of more equilibrium in the mean flow.

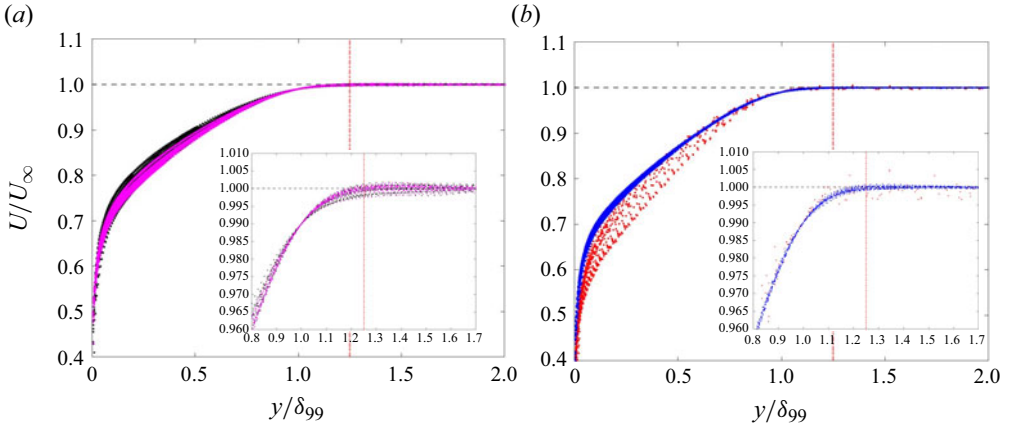

Figure 1. Mean velocity profiles from boundary layers of data sets used (Nagib *et al.* 2004; Sanmiguel Vila *et al.* 2020), normalized by free-stream velocity U_∞ and δ_{99}; (*a*) FPG in magenta and SFPG in black from NDF; (*b*) APG in red from MTL and APG in blue from NDF; dashed red lines at $y/\delta_{99} = 1.25$, corresponding to $\Delta_{1.25}$.

2. Boundary-layer databases

Two sets of boundary-layer data were selected and used because the pressure gradients imposed were well controlled and documented, and independent wall-shear stress was measured directly by oil-film interferometry. One was carried out in the NDF wind tunnel at Illinois Tech (IIT, Chicago) (Nagib, Christophorou & Monkewitz 2004) and the other was obtained in the MTL wind tunnel of KTH (Stockholm) (Sanmiguel Vila *et al.* 2020). Both sets of data were measured by hot-wire anemometry and the free-stream velocity was measured independently using Pitot probe measurements at reference points above the boundary layers developing on a suspended flat plate. In the case of the MTL data we did not use the 'strongly increasing' pressure-gradient data, and only the 30 m s^{-1} cases to avoid any low Re_τ effects and insure fully turbulent conditions even near the start of the boundary-layer development. More cases were studied by Sanmiguel Vila *et al.* (2020).

The velocity profiles of all the data used by us are shown in figure 1. Since the work by Chauhan, Monkewitz & Nagib (2009), a composite mean velocity profile has been used to determine an outer scale of ZPG boundary layers instead of various other measures of the boundary-layer thickness, including integral thicknesses, e.g. Samie *et al.* (2018) and MN23. This outer scale δ was systematically compared with the large data base used by Chauhan *et al.* (2009), and we concluded that for ZPG, $\delta \approx 1.25\delta_{99}$. In both the NDF and MTL data sets we used, we also found that approximate measure of an outer scale to the edge of the boundary layers is valid under APG, FPG and SFPG conditions in addition to ZPG. Therefore, we utilized the outer scale $\ell \equiv \Delta_{1.25} = 1.25\delta_{99}$, and $\beta \equiv (-\Delta_{1.25}/\tau_w) \cdot (\partial P_e/\partial x)$. We also define $Y \equiv y^+/Re_\tau$ to obtain the following from (1.2):

$$U^+_{x_{OL}}(Y \ll 1) \sim \kappa^{-1} \ln Y + \kappa^{-1} \ln Re_\tau + S_0 Y + B_0 + B_1/Re_\tau. \tag{2.1}$$

Simplifying, we obtain

$$U^+_{x_{OL}}(Y \ll 1) = \kappa^{-1} \ln Y + \kappa^{-1} \ln Re_\tau + S_0 Y + B_0 + HOT. \tag{2.2}$$

With increasing Reynolds number, the higher-order terms (HOT) starting with B_1/Re_τ may be ignored. The pressure-gradient parameter defined using the outer scale $\Delta_{1.25}$

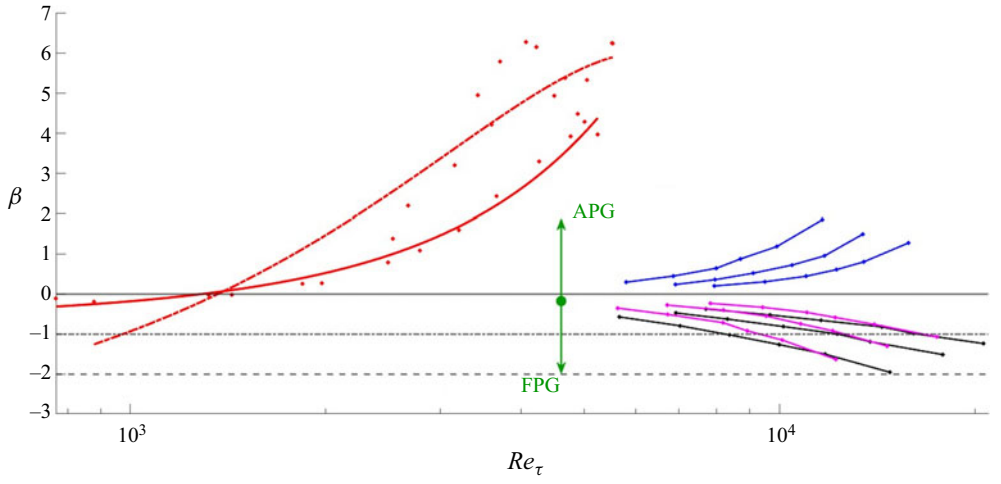

Figure 2. Reynolds-number dependence of pressure-gradient parameter, β, in boundary layers of data sets used; APG data in red dots with second-order best fit for two configurations in MTL by Sanmiguel Vila *et al.* (2020), 'mildly increasing' APG (dotted red line) and 'approximately constant' APG (red line); data from NDF by Nagib *et al.* (2004) for three configurations at six streamwise locations and three free-stream velocities: FPG in magenta, SFPG in black and APG in blue; black lines depict ZPG (solid) fully developed channel (dotted) and fully developed pipe (dashed) conditions.

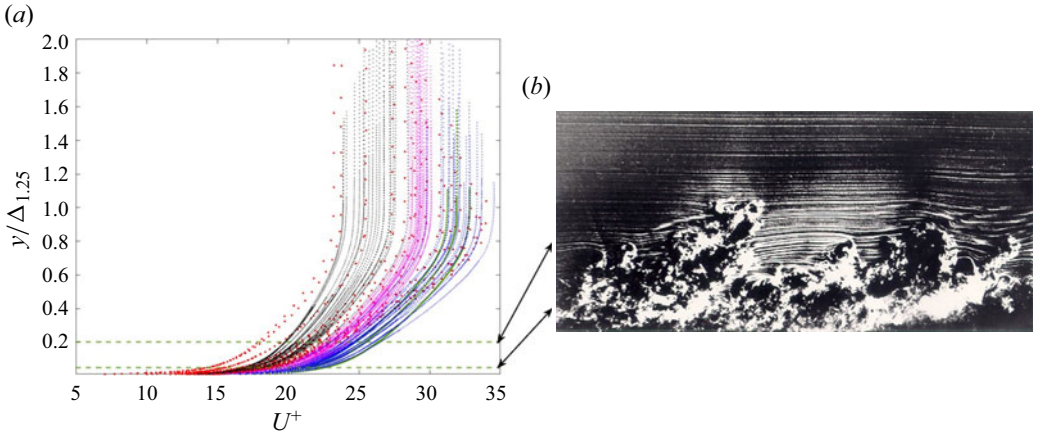

Figure 3. (*a*) Inner-scaled mean velocity profiles plotted on linear scales against $y/\Delta_{1.25}$ for boundary layers of data sets used: FPG (magenta), SFPG (black), ZPG (green), and APG (blue) from NDF, and APG (red) from MTL; dashed green lines at $y/\Delta_{1.25} = 0.05$ and 0.2 correspond to dashed green lines in figure 4; (*b*) smoke-wire visualization of ZPG boundary layer in NDF at Re_θ, which is the Reynolds number based on momentum thickness, and is around 1800 with arrows corresponding to approximate locations of $y/\Delta_{1.25} = 0.05$ and 0.2.

calculated for all profiles of boundary layers from the NDF and MTL data sets are displayed in figure 2. Note that in figure 3 of Sanmiguel Vila *et al.* (2020) the pressure-gradient parameter used was β^* utilizing δ^* as a length scale and yielding conditions of 'approximately constant' or 'mildly increasing' APG. With the closely spaced data in the range around $0.99U_\infty$, and well into the free stream from the NDF wind tunnel (see figure 3), which included the full APG, ZPG, FPG and SFPG cases, the $\Delta_{1.25}$ was far more reliable than experienced in the literature, and represented more physical thicknesses than for example the Clauser thickness.

Finally, the commonly used indicator function based on the mean velocity profile for wall-bounded turbulence, Ξ, can be obtained from

$$\Xi = y^+ \frac{\mathrm{d}U_x^+}{\mathrm{d}y^+} = Y \frac{\mathrm{d}U_x^+}{\mathrm{d}Y}. \tag{2.3}$$

From (2.3) it can be noted that Ξ takes a constant value if a pure logarithmic region of the form (1.1) is present in the mean velocity profile. Furthermore, from (2.2) and (2.3), one can obtain the equation for κ and S_0:

$$\Xi_{OL} = \kappa^{-1} + S_0 y^+ / Re_\tau = \kappa^{-1} + S_0 Y. \tag{2.4}$$

3. Determining overlap coefficients

Applying (2.3) to mean-velocity-profile data of any wall-bounded flow in inner or outer distances from the wall, y^+ or Y, respectively, can result in determining κ and S_0 by a linear fit corresponding to (2.4). One needs to only select the range in y^+ or Y to fit the linear relations. In figure 3(*b*) of Lee & Moser (2015), for $Re_\tau \approx 5200$, they applied a linear fit over around $300 < y^+ < 700$ ($0.06 < Y < 0.14$) and obtained $\kappa = 0.384$ and $S_0 = 0$. Instead, if they had applied a linear fit over $0.21 < Y < 0.45$ ($1100 < y^+ < 2300$), they would have obtained $\kappa = 0.41$ and $S_0 = 1.11$, which compare very well with values for channel flows obtained by MN23, i.e. $\kappa = 0.417$ and $S_0 = 1.1$. Recently, Hoyas *et al.* (2023) obtained values of $\kappa = 0.51$ and $S_0 = 2.6$ also for channel flows computed with two different resolutions using this approach over $0.3 < Y < 0.6$ for $Re_\tau = 550$. The value of $B_0 = 6.9$ was then obtained using the already determined values of κ and S_0 by minimizing the differences between the velocity profile data to (2.2).

This approach requires highly accurate and closely spaced data for the velocity profiles to apply the derivatives of the indicator function Ξ. This is often the case from direct-numerical-simulation (DNS) data, and to some degree in the boundary-layer data from the NDF, where over 200 data points with equal physical spacing were measured. Typical wall-bounded-flow measurements, including in boundary layers, collect the measurements using points with logarithmic physical spacing, i.e. with increasing physical separation away from the wall. This has been a tradition based on an expected 'log law' in the overlap region. The MTL data set was obtained in this way with only 45 to 75 measurement points in the wall-normal direction. The profiles of figure 3 display the measured points and demonstrate the contrast in spacing between MTL (red) and NDF (blue, green, magenta and black). While determining the indicator function Ξ from the MTL data was attempted using several ways, it was found to be not reliable and produced noisy results. On the other hand, two examples of Ξ obtained from NDF profiles are shown in figure 4. To process both data sets using the same approach and algorithms, a different method was required. However, the Ξ profiles from all of the NDF data were very important to select the range of Y to use for the overlap region. Based on the experience from MN223 and Hoyas *et al.* (2023), it is found that fitting in the outer-scaled distances Y from the wall is more representative of the overlap region than by using inner-scaled distances y^+, over wider ranges of Re_τ. It also helps in avoiding the wake region especially for APG conditions, and other pressure-gradient boundary layers, including ZPG.

The approach used here is different from that for channel and pipe flows described above as we are retrieving all three parameters of (2.2) at the same time, by utilizing all profiles in U^+ vs Y ($= y/\Delta_{1.25}$). After choosing the limits of the overlap region in Y, we compute the best combination of parameters using nonlinear least-squares curve fitting. We fit our function to the data by adjusting the parameters of the function to minimize the sum of

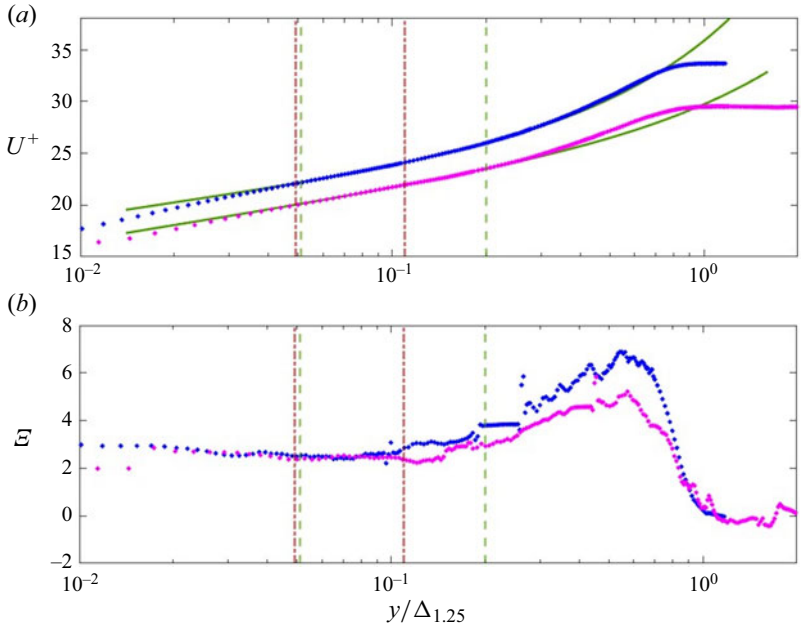

Figure 4. (*a*) Inner-scaled mean-velocity-profile data plotted against logarithmic-scaled $y/\Delta_{1.25}$ for two boundary layers from NDF, for FPG (magenta) and APG (blue); green lines represent the log+lin fit of the overlap region between two vertical dashed green lines at $y/\Delta_{1.25} = 0.05$ and 0.2, and vertical dashed red lines correspond to $y/\Delta_{1.25} = 0.05$ and 0.11, which is consistent with MN23; (*b*) indicator function, Ξ plotted against same scale of (*a*).

squared differences between the observed and predicted values. This optimization involves minimizing the sum of squared residuals.

Given the set of data points $(Y_i,\ U_i^+)$ and the model function $f(\kappa, S_0, B_0, Y_i)$, represented by (2.2), we approximate the combination of parameters that minimizes the difference between the equation and the data for each mean velocity profile: $\forall N \in \mathbb{N}^*$, $(\kappa_{opt}, S_{0_{opt}}, B_{0_{opt}}) = \underset{\kappa,S_0,B_0}{\operatorname{argmin}} \sum_{n=1}^{N} (U_i^+ - f(\kappa, S_0, B_0, Y_i))^2$. This optimization algorithm, with an accuracy of the order of 10^{-8}, leads to the final values of the three parameters of the log+lin overlap for each velocity profile, using $Y_{min} = 0.05$ and $Y_{max} = 0.2$.

4. Discussion and conclusion

With the approach described in the last part of the previous section, a parametric evaluation of the range of Y to extract the parameters of the log+lin overlap from the mean-velocity-profile data was conducted using the NDF data first and then extended to the MTL profiles to arrive at a single range for all data. The choice of these values in our analysis is motivated by the important role of intermittency in boundary layers. This aspect is critical in particular in the presence of pressure gradients. For pipe and channel flows our work, not included here but used by Monkewitz & Nagib (2023), reveals a robust range for an overlap region of $0.3 < Y < 0.5$. To avoid the intermittent region primarily beyond $Y > 0.25$, we focused on and used an upper limit of $Y = 0.2$. To exclude the viscous sublayer from the overlap region we recommend and use $Y > 0.05$. This is supported by the experience from MN23, especially for ZPG. For the lower limit $Y_{OL,min}$ we arrived at a value of 0.05 to accommodate the lower range of Re_τ values in the MTL data. For the upper

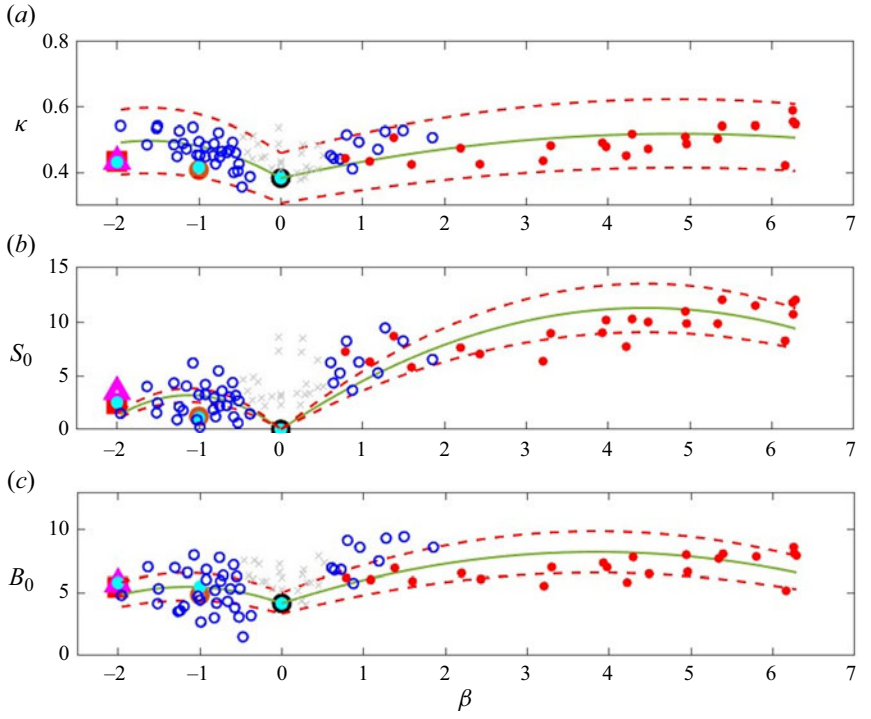

Figure 5. Best-fit overlap parameters, κ, S_0 and B_0 based on (2.2) plotted against pressure-gradient parameter, β, for all data sets of figure 3; NDF in open blue circles and MTL in closed red circles, with ZPG from NDF and Samie *et al.* (2018) in large black open circle; parameter values from Monkewitz & Nagib (2023) in closed cyan circles; parameter values from DNS of Hoyas *et al.* (2023) for channel (large brown open circles) and pipe (large red open square); recent experiments in CICLoPE Pipe in magenta triangle; green lines are second-order best fits of all figure data with dashed red line representing 20 % deviations from fit (see table 1); faint grey crosses represent profiles with high fit uncertainty.

limit of the range $Y_{OL,max}$, we tested several values in the range $0.11 < Y < 0.4$ (compare with figure 7 of MN23). Based on both sets of data, and in order to avoid including parts of the wake, which varies with pressure gradient, we again converged on $Y_{OL,max} = 0.2$. Two ranges are indicated in figure 4 with dashed lines representing $Y_{OL,min} = 0.05$ and $Y_{OL,max} = 0.11$ in red, and $Y_{OL,min} = 0.05$ and $Y_{OL,max} = 0.2$ in green. The resulting log+lin overlap fit based on (2.4) is shown in solid curves, also in green, with the mean velocity profiles corresponding to an FPG case and an APG case. Note that for the FPG case with the smaller wake, as indicated by the Ξ curves, the profile data are above the log+lin overlap fit beyond $Y > 0.3$. Further systematic study of the best choice may lead to an ultimate best value of $Y_{OL,max}$ and its possible dependence on pressure gradient, but we are satisfied with the 0.2 value especially in light of the results presented in figures 5 and 6.

Boundary layers with small pressure gradients $-0.5 < \beta < 0.5$, including ZPGs, are the most sensitive to the choice of $Y_{OL,max}$ for the accurate extraction of the log+lin overlap parameters and in particular S_0, because of the influence of the wake part. These profiles come from a mixture of NDF cases and the MTL cases, with the fewer data points in the profile, and the resulting parameters are included in figure 5 with grey crosses. The discrimination between the log+lin overlap region and the start of the outer-wake region requires closely spaced measurement points.

Favourable pressure gradient	Adverse pressure gradient
$\kappa_- = -0.044\,\beta^2 - 0.142\,\beta + 0.384$	$\kappa_+ = -0.006\,\beta^2 + 0.056\,\beta + 0.384$
$S_{0_-} = -2.516\,\beta^2 - 5.652\,\beta$	$S_{0_+} = -0.569\,\beta^2 + 5.068\,\beta$
$B_{0_-} = -0.974\,\beta^2 - 2.261\,\beta + 4.17$	$B_{0_+} = -0.275\,\beta^2 + 2.114\,\beta + 4.17$

Table 1. Equations for second-order best fits of overlap parameters, κ, S_0 and B_0, for NDF and MTL Data.

In figure 3(*a*), we included the selected values $Y_{OL,min} = 0.05$ and $Y_{OL,max} = 0.2$ on the velocity profiles also in green dashed lines. The arrows starting from those values of $Y = y/\Delta_{1.25}$ to the upstream edge of the flow-visualization image in figure 3(*b*) are intended to point to the approximate corresponding distances from the wall at the bottom of the image.

All the data for best-fit values of κ, S_0 and B_0 for each boundary-layer velocity profile from both datasets are included in figure 5. Furthermore, data from MN23, Samie *et al.* (2018) and Hoyas *et al.* (2023) are added to the figure. It is important to point out that MN23 defined their pressure-gradient parameter β without a minus sign so pipe and channel flows were represented by positive values of β. All the data in each part of figure 5 were used to fit second-order polynomials, using an algorithm to minimize the differences with an accuracy of the order of 10^{-3}, resulting in the summary of table 1.

A correlation to test the universality of the Kármán coefficient was developed by Nagib & Chauhan (2008) and is shown by their equation (13), which was based on a log-only overlap region:

$$\kappa B = 1.6\,[e^{0.1663B} - 1]. \tag{4.1}$$

For a constant or universal Kármán constant, κ, a linear relation between κB and B needs to exist. In figure 6 we test the universality of κ based on the log+lin overlap region and plot all the data from both sets. Lines of various values of constant κ are included for reference and none of them represent the entire data sets or segments of them with any reasonable accuracy. Fitting the data extracted using the log+lin overlap by a similar relation to (2.2) we find, using an algorithm to minimize the differences with an accuracy of the order of 10^{-3}, slightly different coefficients in the relation:

$$\kappa B_0 = 4.05\,[e^{0.087B_0} - 1]. \tag{4.2}$$

Based on the results of figure 5, we conclude that when using the log+lin overlap given by (2.2), no history effects are observed in the overlap region in either of the two data sets used here or between them, over a very wide range of Reynolds numbers, APGs and FPGs. We interpret this behaviour as quasiequilibrium of the overlap between outer and inner parts when the new understanding of the overlap region of Monkewitz & Nagib (2023) is adopted. In the literature, some history effects have been observed in pressure-gradient boundary layers but in the well-documented studies (Harun *et al.* 2013; Bobke *et al.* 2017) they are reflected primarily in Reynolds stresses or the wake part of the mean flow. We only used the approximately constant and mildly increasing pressure gradient cases from MTL. Sanmiguel Vila *et al.* (2020) data included a strongly increasing case with β^* up to 2.38. The validity of our conclusions on the history effects will need to be examined for a wider range of β as defined here with an outer length scale. Note that the new understanding of the overlap region developed by Monkewitz & Nagib (2023), and utilized here over a wide range of pressure-gradient boundary layers, can contribute to the development of novel modelling strategies for turbulence, as well as to enhanced correlations to predict, e.g. the

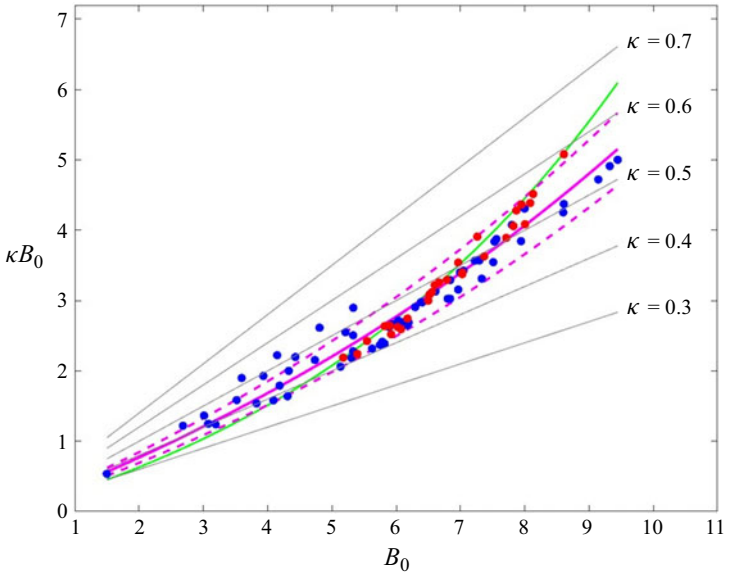

Figure 6. Product of κB_0 plotted against B_0 to test universality of Kármán coefficient against lines of constant κ based on best-fit overlap parameters from (2.2); NDF data in blue dots and MTL data in red dots; magenta line is best fit according to (4.2) with 10 % deviation indicated by dashed lines; green curve is similar fit of a wide range of data using composite profiles by Nagib & Chauhan (2008) for a log-only overlap region, shown in (4.1).

skin friction of turbulent boundary layers subjected to various pressure gradients. It has already clarified differences between wall-bounded flows in pipes, channels and boundary layers. The contrast between the influence of the outer flow or wake region on the overlap region is far more pronounced when utilizing the log+lin overlap compared with the pure log interpretation of the overlap region.

Acknowledgements. V.B. and H.N. acknowledge the ongoing support of the J.T. Rettaliata Chair of Mechanical and Aerospace Engineering. R.V. acknowledges the financial support from ERC grant no. 2021-CoG-101043998, DEEPCONTROL. Views and opinions expressed are, however, those of the authors only and do not necessarily reflect those of the European Union or European Research Council. Neither the European Union nor granting authority can be held responsible for them.

Declaration of interests. The authors report no conflict of interest.

Author ORCIDs.
Ricardo Vinuesa https://orcid.org/0000-0001-6570-5499;
Hassan Nagib https://orcid.org/0000-0002-4530-9920.

References

Afzal, N. & Yajnik, K. 1973 Analysis of turbulent pipe and channel flows in moderately large Reynolds numbers. *J. Fluid Mech.* **61**, 23–31.

Bobke, A., Vinuesa, R., Örlü, R. & Schlatter, P. 2017 History effects and near equilibrium in adverse-pressure-gradient turbulent boundary layers. *J. Fluid Mech.* **820**, 667–692.

Chauhan, K., Monkewitz, P. & Nagib, H. 2009 Criteria for assessing experiments in zero pressure gradient boundary layers. *Fluid Dyn. Res.* **41**, 021404.

George, W.K. & Castillo, L. 2006 Recent advancements toward the understanding of turbulent boundary layers. *AIAA J.* **44**, 2435–2449.

HARUN, Z., MONTY, J.P., MATHIS, R. & MARUSIC, I. 2013 Pressure gradient effects on the large-scale structure of turbulent boundary layers. *J. Fluid Mech.* **715**, 477–498.

HOYAS, S., VINUESA, R., BAXERRAS, V. & NAGIB, H. 2023 Resolution and convergence requirements for extended overlap region in wall-bounded turbulence. arXiv:2311.05204v1 [physics.flu-dyn], pp. 1–6.

LEE, M. & MOSER, R. 2015 Direct numerical simulation of turbulent channel flow up to $Re_\tau \approx 5200$. *J. Fluid Mech.* **774**, 395–415.

LUCHINI, P. 2017 Universality of the turbulent velocity profile. *Phys. Rev. Lett.* **118**, 224501.

MONKEWITZ, P.A., CHAUHAN, K.A. & NAGIB, H.M. 2008 Comparison of mean flow similarity laws in zero pressure gradient turbulent boundary layers. *Phys. Fluids* **20**, 105102.

MONKEWITZ, P.A. & NAGIB, H.M. 2023 The hunt for the Kármán 'constant' revisited. *J. Fluid Mech.* **967**, A15.

NAGIB, H.M. & CHAUHAN, K.A. 2008 Variations of von Kármán coefficient in canonical flows. *Phys. Fluids* **20**, 101518.

NAGIB, H.M., CHRISTOPHOROU, C. & MONKEWITZ, P.A. 2004 High Reynolds number turbulent boundary layers subjected to various pressure-gradient conditions. In *Proceedings of IUTAM Symposium on One Hundred Years of Boundary Layer Research; Göttingen, Germany* pp. 383–394. Springer.

SAMIE, M., MARUSIC, I., HUTCHINS, N., FU, M.K., FAN, Y., HULTMARK, M. & SMITS, A.J. 2018 Fully resolved measurements of turbulent boundary layer flows up to $Re_\tau = 20\,000$. *J. Fluid Mech.* **851**, 391–415.

SANMIGUEL VILA, C., VINUESA, R., DISCETTI, S., IANIRO, A., SCHLATTER, P. & ÖRLÜ, R. 2020 Resolution and convergence requirements for extended overlap region in wall-bounded turbulence. *Exp. Therm. Fluid Sci.* **112**, 109975.

VINUESA, R., SCHLATTER, P. & NAGIB, H.M. 2014 Role of data uncertainties in identifying the logarithmic region of turbulent boundary layers. *Exp. Fluids* **55**, 1751.

VISHWANATHAN, V., FRITSCH, D.J., LOWE, K.T. & DEVENPORT, W.J. 2023 History effects and wall-similarity of non-equilibrium turbulent boundary layers in varying pressure gradient over rough and smooth surfaces. *Intl J. Heat Fluid Flow* **102**, 109145.

YAJNIK, K. 1970 Asymptotic theory of turbulent shear flows. *J. Fluid Mech.* **42**, 411–427.